Inorganic Chemistry

Article

pubs.acs.org/IC

Zinc Hydroxyacetate and Its Transformation to Nanocrystalline Zinc Oxide

Amir Moezzi, Andrew McDonagh, Annette Dowd, and Michael Cortie*

Institute for Nanoscale Technology, University of Technology Sydney, Sydney, New South Wales 2007, Australia

Supporting Information

ABSTRACT: The synthesis of nanocrystalline ZnO by thermal decomposition of zinc hydroxyacetate, $Zn_5(OH)_8(CH_3CO_2)_2{\cdot}nH_2O$, was investigated. The decomposition process was examined using X-ray diffraction, thermogravimetric analysis, mass spectrometry, electron microscopy, Brunauer–Emmett–Teller surface area analysis, and solid-state NMR spectroscopy. Intermediate $Zn_5(OH)_8(CH_3CO_2)_2{\cdot}nH_2O$ phases form at temperatures up to 110 °C from the starting compound $Zn_5(OH)_8(CH_3CO_2)_2{\cdot}2H_2O$ by partial dehydration. At ~110 °C, 4 equiv of ZnO and 1 equiv of $Zn(CH_3CO_2)_2$ are formed. Further heating causes $Zn(CH_3CO_2)_2$ to decompose to acetone, acetic acid, acetic anhydride, and ZnO. Notably, a portion of $Zn(CH_3CO_2)_2$ sublimes during the process. Overall, the product of the calcination is equiaxed ZnO nanocrystals of 20–100 nm diameter.

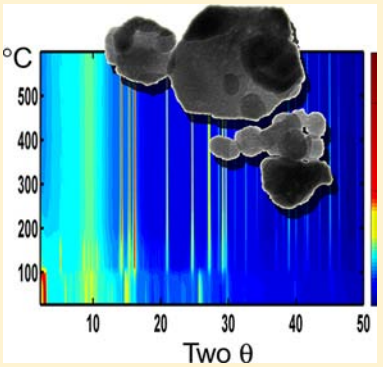

1. INTRODUCTION

Zinc hydroxy salts are important materials with industrial and scientific applications. Zinc hydroxysulfate, for example, is used in pigments and in fertilizers,[1−3] and zinc hydroxynitrate is an esterification catalyst[4,5] and an interesting anion-exchange material.[6] In addition, these compounds are useful precursors for the preparation of zinc oxide (ZnO).[3]

ZnO has numerous existing and potential applications including in the rubber and tire industries, as a catalyst support, as a UV-blocking additive to polymers and cosmetics, as a corrosion-inhibiting pigment for paints, and as a semiconductor with specialized properties for a wide range of electronic or optoelectronic applications.[3,7,8] Most ZnO is produced by high-temperature gas-phase processes that produce material with relatively large particle sizes and low specific surface areas.[3] Alternatively, ZnO may be produced by wet chemical means[9] or by thermal decomposition of zinc-containing precursors. Of particular relevance to the current work is the thermal decomposition of zinc hydroxyacetate, ($Zn_5(OH)_8(CH_3CO_2)_2{\cdot}nH_2O$),[10−15] to form nanocrystalline ZnO and the mechanism by which this process takes place.

$Zn_5(OH)_8(CH_3CO_2)_2{\cdot}nH_2O$ is a layered hydroxide, comprised of sheets of cationic zinc hydroxy species and associated acetate anions.[16,17] The number of waters of crystallization, n, has been reported to be between 1.5 and 4 depending on the synthesis method, with the values for n calculated from thermogravimetric analysis (TGA) mass loss data. Powder X-ray diffraction (XRD) patterns of $Zn_5(OH)_8(CH_3CO_2)_2.nH_2O$ exhibit a strong (001) reflection associated with the interlayer distance between the sheets with $d \approx 1.34$ nm. Second-order (002) and third-order (003) peaks associated with the 001 reflection are located at ~0.67 and ~0.45 nm, respectively. However, there is as much as a ±0.35 nm variation in the reported values of d between various authors, which seems to be related to the synthetic method. This is more than would be anticipated by interlaboratory scatter and is evidently caused by variable composition, which, in turn, affects the structure.[13,16−21]

Several procedures have been reported for the synthesis of zinc hydroxyacetate. These include reaction of a solution of zinc acetate with a base such as sodium hydroxide,[16,22] reaction of ZnO powder with zinc acetate in solution,[11] or an anion exchange reaction between zinc hydroxy chloride and zinc acetate dihydrate.[15] The preparation of $Zn_5(OH)_8(CH_3CO_2)_2{\cdot}nH_2O$ using ammonium hydroxide[12] or in alcoholic media[17,18,23] may be problematic because the inclusion of organic or inorganic materials is possible.[24] A detailed investigation of this latter aspect is currently underway and will be reported by us elsewhere.

Previous works examining the transformation of $Zn_5(OH)_8(CH_3CO_2)_2{\cdot}nH_2O$ to ZnO have found that this material forms nanocrystalline ZnO at moderate temperatures with some intermediate crystalline phases and gaseous products identified.[11,14,22] In this Article, we present the results of our detailed investigation of the synthesis of $Zn_5(OH)_8(CH_3CO_2)_2{\cdot}nH_2O$, an evaluation of the number of waters of hydration, and the mechanism of its transformation by calcination to ZnO. We also provide evidence for the first time for the involvement of a sublimation process during thermal decomposition of zinc hydroxyacetate.

Received: June 15, 2012
Published: December 18, 2012

   dx.doi.org/10.1021/ic302328e | Inorg. Chem. 2013, 52, 95−102

2. EXPERIMENTAL SECTION

2.1. General Procedures. Analytical-reagent-grade zinc acetate dihydrate, zinc oxide (ZnO), and sodium hydroxide pellets were purchased from Ajax Chemicals and used as-received. Milli-Q water was used as the solvent.

Synchrotron powder X-ray diffraction (XRD) studies were performed on $Zn_5(OH)_8(CH_3CO_2)_2{\cdot}nH_2O$ by continuous powder XRD of 0.1-mm-diameter quartz capillaries filled with sample at the Australian Synchrotron. The X-ray wavelength was set at 0.696603 Å (confirmed by refinement on a LaB_6 standard). The time stamp corresponded to the beginning of each 2 min collection interval, and the sample was ramped at 5 °C/min. Three-dimensional (3D) and color-coded contour graphs were generated using *MATLAB* version 7, which was also used for numerical analysis. Intensity data were corrected by division of the intensity figure by the integrated ion chamber count figure multiplied by 10^5 to form an arbitrary unit. Deconvolution of low-angle XRD peaks was undertaken with the free software *Fityk*. XRD experiments of powder samples were also performed using a laboratory Siemens D5000 X-ray diffractometer with a graphite post-monochromator with the following parameters: wavelength 1.5406 Å (Cu Kα), tube power 1.6 kW (40 kV at 40 mA), step size 0.02°, time per step 2 s, divergent slit 1°, receiving slit 0.02 mm, and scan angle range 3−80°, unless otherwise stated. Scanning electron microscopy (SEM) images were obtained using a Zeiss Supra 55VP scanning electron microscope operating in high-vacuum mode. An accelerating voltage of 5−20 kV was used with 10−30 μm aperture, and images were obtained using an in-lens secondary detector. Thermogravimetric analysis (TGA) experiments were performed using TA Instruments SDT 2960 with simultaneous differential thermal analysis (DTA)−TGA. A heating rate of 5 °C/min was used in an air atmosphere. Simultaneous TGA−mass spectrometry (MS) experiments were conducted using a Quadrupole mass spectrometer (model Thermostar QMS 200 M3) from Balzers Instruments in a platinum crucible. The current intensities associated with the following masses were examined: CO_2, 44; H_2O, 18; O_2, 32; acetic acid, 60; acetone, 58; acetic anhydride, 102. Brunauer−Emmett−Teller (BET) specific surface area measurement was performed using Autosorb-1 from Quantachrome Instrument by the precise vacuum volumetric method for nitrogen chemisorption. Multipoint (five points) measurement was conducted on the sample. Cross-polarization magic-angle-spinning (CPMAS) ^{13}C NMR spectra were recorded using a Bruker 200 MHz NMR spectrometer operating at 50 MHz. The sample was loaded into a 4-mm zirconium oxide rotor with a Kel-F cap and spun at 5000 Hz. A pulse width of 4.5 μs was used with a contact time of 2 ms. In total, 485 scans were collected. Free induction decay signals were obtained during a 0.05 s acquisition time, followed by a 5 s delay. Chemical shifts were measured with respect to adamantane as the external standard at 38.48 ppm.

2.2. Synthesis of Zinc Hydroxyacetate Dihydrate. *Method A.*

$$8NaOH(aq) + 5Zn(CH_3CO_2)_2{\cdot}2H_2O(aq) \rightarrow Zn_5(OH)_8(CH_3CO_2)_2{\cdot}2H_2O(s) + 8Na(CH_3COO)(aq) + 10H_2O \quad (1)$$

Aqueous solutions of zinc acetate (60 mL, 1.5 M, pH 6) and sodium hydroxide (60 mL, 1.5 M, pH 14) were rapidly mixed at room temperature in a round-bottomed flask. The mixture was stirred for 2 h, after which the pH was 7. The white precipitate was collected by vacuum filtration, washed with water, and dried overnight in an oven set at 60 °C. The powder was characterized by powder XRD, ^{13}C NMR, and TGA. A portion of the powder was calcined in a preheated oven at 400 °C for 2 h, after which it was allowed to cool under natural convection to room temperature and analyzed ex situ.

Method B. An aqueous solution of zinc acetate (60 mL, 1.5 M, 0.09 mol) was added to ZnO powder (0.09 mol) suspended in 60 mL of water in a single step. The mixture was stirred for between 1 and 24 h at room temperature. The white suspension was then filtered and washed with water. Samples that were dried were placed in an oven at 60 °C overnight. Undried samples were not subjected to temperatures greater than room temperature. For the TGA−DTA test, a sample was dried at room temperature under vacuum overnight.

3. RESULTS AND DISCUSSION

Figure 1 shows the powder XRD patterns of the method A and B products, as dried at various temperatures. These patterns are

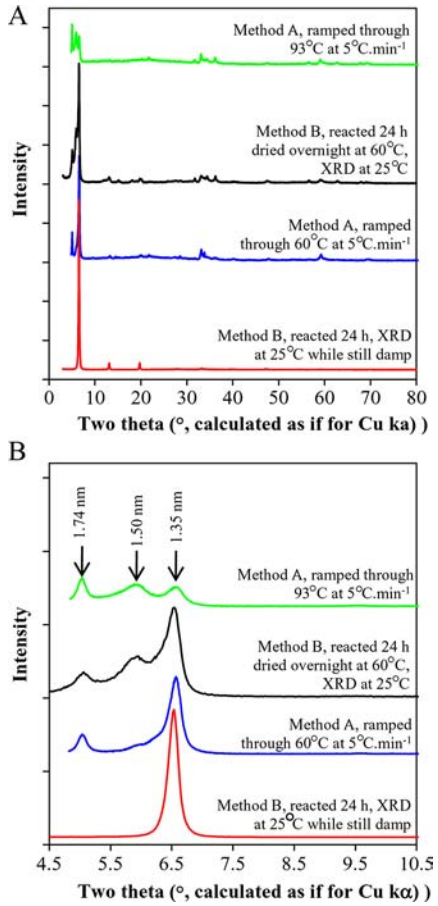

Figure 1. X-ray diffractograms (synchrotron radiation) of as-synthesized zinc hydroxyacetate. All 2θ was converted to be equivalent to Cu Kα for ease of comparison. (a) Whole scan. (b) Magnified view of the low-angle region showing the presence of three distinct peaks, each corresponding to a phase with a unique interlayer spacing.

similar to XRD patterns for compounds reported as $Zn_5(OH)_8(CH_3CO_2)_2{\cdot}nH_2O$, where n = 2,[10,25] ~3,[15,26] or 4.[11,22] The most intense (001) peak in Figure 1 corresponds to an interlayer d spacing of ~1.35 nm at room temperature. Second-order (002) and third-order (003) peaks associated with the 001 reflection correspond to d spacings of 0.67 and 0.44 nm, respectively. However, overlapping peaks were observed at low values of 2θ for some of the samples. Deconvolution of the raw data in those instances revealed peaks corresponding to d spacings of ~1.35, ~1.50, and ~1.75 nm (see the Supporting Information). Given that each compound can only manifest one kind of (001) interlamellar diffraction peak apiece, it follows that there must be up to three layered compounds present in these samples. Peaks of this nature have also been previously reported by others for this class of material,[13,16,19−21] although in some cases, the presence of two peaks has been attributed to the presence of a "bilamellar" crystal structure.[26] However, even a "bilamellar" structure

dx.doi.org/10.1021/ic302328e | *Inorg. Chem.* 2013, 52, 95−102

should only generate a single XRD peak, corresponding to the repeat distance of the periodic bilamellar motif.

Only one peak (001) in the low-angle region (d = 1.35 nm) is evident in the well-aged method B material (damp and at room temperature), with the associated second- and third-order peaks centered at d = 0.68 and 0.45 nm, respectively, indicating a single phase. In contrast, samples obtained after only 1 h or after 24 h of reaction but dried overnight at 60 °C exhibit multiple low-angle peaks similar to those observed in the data for the material prepared using method A (which was dried at 60 °C; see the Supporting Information). This shows that the structure is quite sensitive to drying even at relatively low temperatures. The data indicate that, as the temperature is increased and the degree of hydration is reduced, the phases replace one another in the sequence d = ∼1.35 nm, then d = ∼1.50 nm, and then d = ∼1.75 nm. The effect of the temperature is discussed in detail below.

TGA experiments on the products of methods A and B showed mass losses of 37.4% and 39.7% upon heating to 1000 °C, respectively (see the Supporting Information). These would ostensibly suggest that n = 4 if all of the mass loss was due to decomposition of zinc hydroxyacetate to ZnO only (the theoretical mass loss upon complete conversion to ZnO is 37.7% if n = 4 and 34.0% if n = 2). This conclusion has been drawn by some previous workers in the field.[11,22] However, as we show later, the samples contain unbound water (0.9% and 3.2%, respectively) at temperatures below ∼60 °C, while, in addition, thermal decomposition at higher temperatures releases some volatile zinc species, calculated to be responsible for a mass loss of ∼1.8−2.9%. Taking these factors into consideration, an actual mass loss in the range of 33.6−34.7% indicates that n = 2 to give the chemical formula of $Zn_5(OH)_8(CH_3CO_2)_2{\cdot}2H_2O$. This conclusion is in agreement with the work of Cui et al.[12] and Morioka et al.[16]

It has been suggested [based on Fourier transform infrared (FTIR) spectroscopy] that the bonding of the acetate anions to zinc cations in the interlayer space is purely ionic[22] or unidentate and chelating.[19,26] However, it has also been reported that FTIR data alone may be insufficient to ascertain the coordination mode of the carboxylate groups.[27] To investigate the nature of the acetate bonding in these structures, CPMAS ^{13}C NMR spectra for the product of method A were recorded (Figure 2). This technique has proven useful to distinguish acetate/metal coordination modes.[27] Two signals assigned to resonances of the carbon atoms associated with the CH_3 and COO groups were observed at 25 and 180 ppm, respectively. A comparison with the CPMAS ^{13}C NMR chemical shifts of the carbonyl groups in related zinc compounds bearing carboxylate groups[27] suggests that the acetate group is coordinated in a bidentate bridging fashion. The chemical shift recorded in the current work is inconsistent with the assignment of a chelating, unidentate, or ionic bonding mode.[27−29]

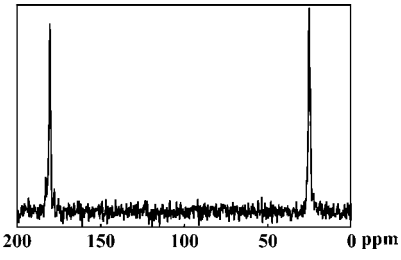

Figure 2. CPMAS ^{13}C NMR spectrum of $Zn_5(OH)_8(CH_3CO_2)_2{\cdot}2H_2O$ made by method A showing resonances associated with the CH_3 and C═O groups.

Samples of $Zn_5(OH)_8(CH_3CO_2)_2{\cdot}2H_2O$ produced by method A were calcined at 400 °C for 2 h and examined using XRD, BET, SEM, and transmission electron microscopy (TEM). The XRD pattern was consistent with that of ZnO, and no other diffraction peaks were present. A BET specific surface area of 15.4 m^2/g was recorded.

Figure 3 shows SEM images of the $Zn_5(OH)_8(CH_3CO_2)_2{\cdot}2H_2O$ powder and the resultant ZnO particles after calcination. Before calcination, $Zn_5(OH)_8(CH_3CO_2)_2{\cdot}2H_2O$ consists of platelike structures with sizes on the order of micrometers. In contrast, ZnO obtained by calcination of $Zn_5(OH)_8(CH_3CO_2)_2{\cdot}2H_2O$ consists of nanoparticles. TEM images (Figure 4) reveal that the diameters of the individual ZnO crystals are in the range 20−100 nm (average = 41.1 nm, s = 21.1 nm, n = 111 crystals, each measured in two directions).

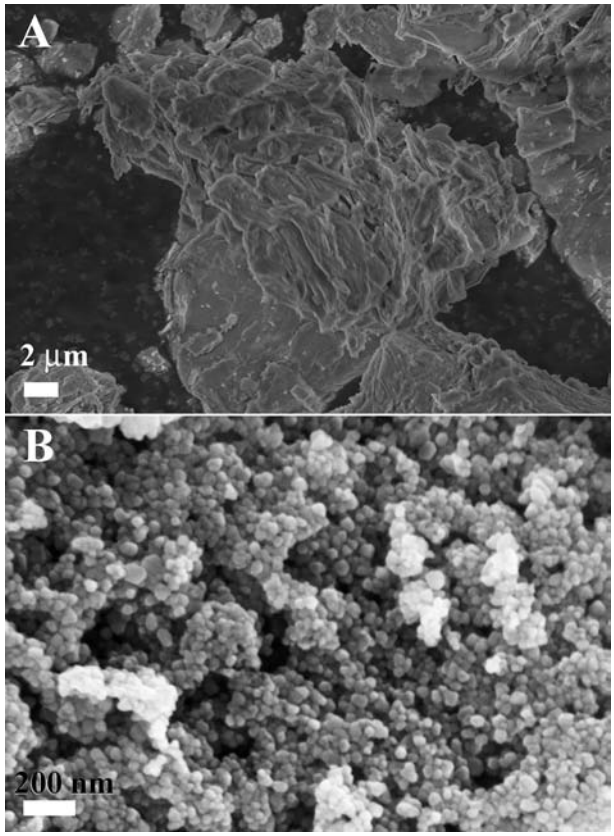

Figure 3. SEM images of (A) $Zn_5(OH)_8(CH_3CO_2)_2{\cdot}2H_2O$ and (B) the calcination product, ZnO.

The next phase of our work sought to examine the transition of $Zn_5(OH)_8(CH_3CO_2)_2{\cdot}2H_2O$ to ZnO in more detail. First, the calcination process was investigated by collecting in situ, real-time XRD patterns using synchrotron radiation, while the $Zn_5(OH)_8(CH_3CO_2)_2{\cdot}2H_2O$ sample (made via method A) was heated from room temperature to 600 °C (Figure 5). Between 68 and 113 °C, there is a marked change in the intensities of the low-angle peaks, indicating a change in the structure of the crystalline material. At 93 °C, peaks assigned to ZnO become evident. At ∼113 °C, a crystalline phase identified as anhydrous

dx.doi.org/10.1021/ic302328e | Inorg. Chem. 2013, 52, 95−102

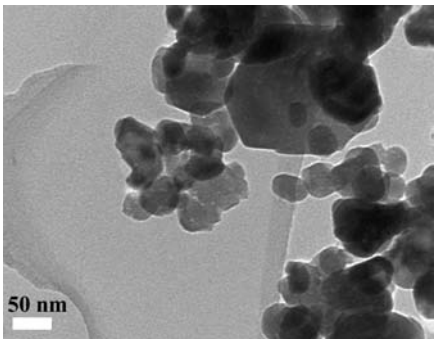

Figure 4. TEM images of the ZnO nanocrystals formed by calcination at 400 °C. The characteristic hexagonal crystal habit of ZnO is clearly visible in some of the larger particles.

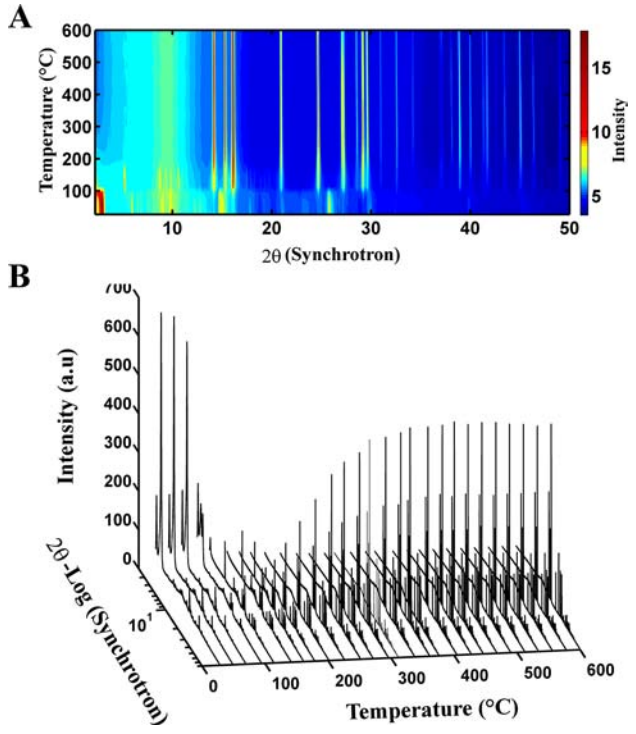

Figure 5. (A) Color-coded contour graph showing powder XRD data collected from the zinc hydroxyacetate sample during in situ experiment between 27 and 600 °C. (B) Sequence of XRD patterns showing the development of diffraction peaks associated with ZnO.

zinc acetate (JC-PDF 00-001-0089) appears. The presence of this phase during thermal decomposition of zinc hydroxyacetate was also deduced by Biswick et al.,[22] who commented that two overlapping thermal processes occur between 50 and 160 °C, which they attributed to the formation of $Zn_5(OH)_8(CH_3CO_2)_2$ and a material tentatively identified as $Zn_3(OH)_4(CH_3CO_2)_2$, which, in turn, decomposed to $Zn(CH_3CO_2)_2$. In our in situ XRD experiments, no diffraction pattern for $Zn_3(OH)_4(CH_3CO_2)_2$ was evident, although we could identify peaks corresponding to those reported for this material in ex situ XRD experiments on material obtained by heating $Zn_5(OH)_8(CH_3CO_2)_2{\cdot}2H_2O$ at 90 °C for 1 h (see the Supporting Information). This finding indicates that the heating rate may significantly affect the formation of intermediate phases. Above 200 °C, only diffraction patterns associated with ZnO were observed.

Figure 6 shows the integrated area of a representative peak selected from each of the phases observed in the XRD data,

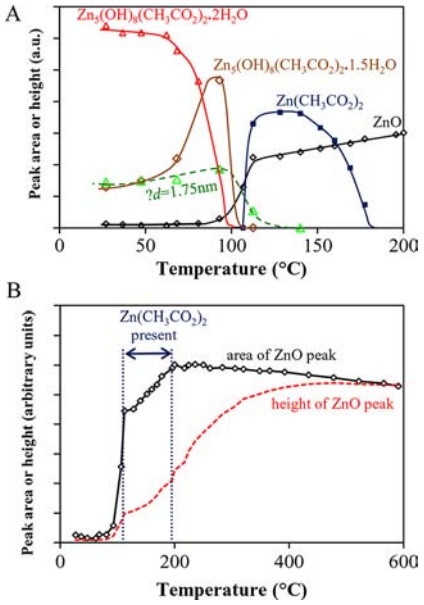

Figure 6. Integrated areas of selected diffraction peaks during the synchrotron experiment. The deconvolutions used to extract the peak areas were performed with the program *Fityk* and up to four pseudo-Voight functions at a time. (A) Evolution of low-temperature phases. (B) Development of the area and height of the peak for ZnO. The region over which $Zn(CH_3CO_2)_2$ was detected is shown by dotted lines. Lines are drawn as a guide to the eye.

plotted against temperature. The peak for d = ~1.35−1.40 nm disappears above 68 °C followed by the disappearance of the peak (or peaks) for d = ~1.45−1.50 nm at about 95 °C. The former peak is clearly from the $Zn_5(OH)_8(CH_3CO_2)_2{\cdot}2H_2O$ phase already identified in the prior literature.[10,16,25] The latter peak is very likely due to the $Zn_5(OH)_8(CH_3CO_2)_2{\cdot}1.5H_2O$ phase[18] (JC-PDF 00-056-0569). The peak for d = 1.75 nm is still strong at 113 °C but disappears above that temperature. The phase responsible for this peak is as yet unidentified. A peak assigned to $Zn(CH_3CO_2)_2$ appears at ~110 °C and reaches its maximum area at ~140 °C.

Interestingly, ~80% of the total ZnO is formed between 90 and 110 °C. There are no peaks attributable to $Zn(CH_3CO_2)_2$ in the XRD patterns obtained at temperatures >200 °C. Beyond this temperature, the integrated *area* of the selected ZnO peak does not change much, although a slight decrease is evident (Figure 6) because of thermal effects that reduce the intensity of the diffraction pattern. However, the *height* of this ZnO peak continues to increase to about 500 °C, indicating that ZnO crystallites are growing and/or annealing, which decreases the width of the XRD peak.

It is important to note that about 80% of the total ZnO is generated *prior* to the formation of $Zn(CH_3CO_2)_2$ and only about 20% comes from subsequent decomposition of that compound. This is quite different from the possibility raised by Biswick et al.[22] in which a new phase, thought to be $Zn_3(OH)_4(CH_3CO_2)_2$, was formed, or from the work of Kandare et al.,[11] who proposed that $Zn_5(OH)_8(CH_3CO_2)_2$ remained stable in excess of 250 °C (we note, however, that a heating rate of 20 °C/min was employed in the latter work). Moreover, in the former case, more than 45 min was required

dx.doi.org/10.1021/ic302328e | *Inorg. Chem.* 2013, 52, 95−102

at 100 °C to form the proposed $Zn_3(OH)_4(CH_3CO_2)_2$ compound, whereas in our continuously ramped experiment, there is evidently insufficient time to form this phase.

Calcination of $Zn_5(OH)_8(CH_3CO_2)_2{\cdot}2H_2O$ made via method A was also examined by TGA–DTA (Figure 7).

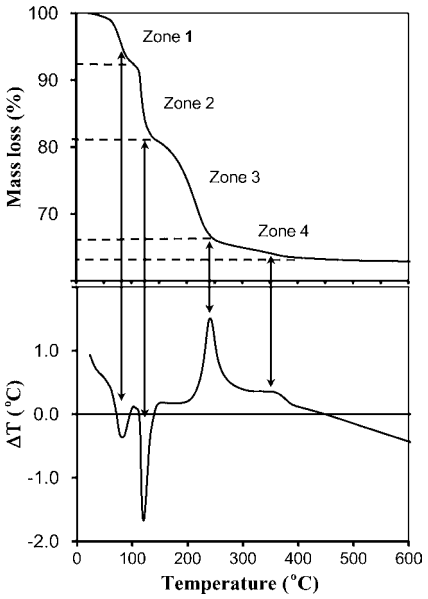

Figure 7. TGA (top) and DTA (bottom) on $Zn_5(OH)_8(CH_3CO_2)_2{\cdot}2H_2O$ made by method A in air at 5 °C/min.

Features in the TGA–DTA data have been assigned as zones to facilitate discussion. Prior to 60 °C, a 0.9% mass loss was observed, which is assigned to the release of surface moisture. Endothermic processes in zone 1 (60–93 °C) associated with a 5.8% mass loss and in zone 2 (93–147 °C) associated with a 12.3% mass loss have a combined mass loss of 18.1%, which is close to the theoretical mass loss (17.5%) ascribed to the release of six water molecules from the formula unit [total of H_2O generated in reactions (2) and (3)]. The mass loss in zone 3 (147–250 °C) of 14.7% and its associated exotherm at 242 °C is assigned to decomposition of $Zn(CH_3CO_2)_2$. At 362 °C, a broad exothermic peak was detected that is associated with 2.7% mass loss between 250 and 400 °C.

$$Zn_5(OH)_8(CH_3CO_2)_2{\cdot}2H_2O \xrightarrow{68-93\ ^\circ C} Zn_5(OH)_8(CH_3CO_2)_2 + 2H_2O \quad (2)$$

$$Zn_5(OH)_8(CH_3CO_2)_2 \xrightarrow{110-200\ ^\circ C} 4ZnO + Zn(CH_3CO_2)_2(s) + 4H_2O \quad (3)$$

Calcination of $Zn_5(OH)_8(CH_3CO_2)_2{\cdot}2H_2O$ made via method B was also examined by TGA–DTA (Supporting Information). TGA reveals a total mass loss of 39.7% between room temperature and 1000 °C including ~3.2% mass loss between room temperature and 60 °C, which is attributed to moisture removal, and around 4% mass loss between 250 and 400 °C. Thus, the total mass losses (on a dried basis) for the materials made from methods A and B are similar. The presence or absence of the exotherm at ~240 °C is somewhat stochastic and, in our experience, is more likely to occur for faster heating rates (e.g., 5 °C/min) than for slower (1 °C/min).

TGA–MS was used to examine the gases evolved during heating (Figure 8). Water was detected at temperatures below

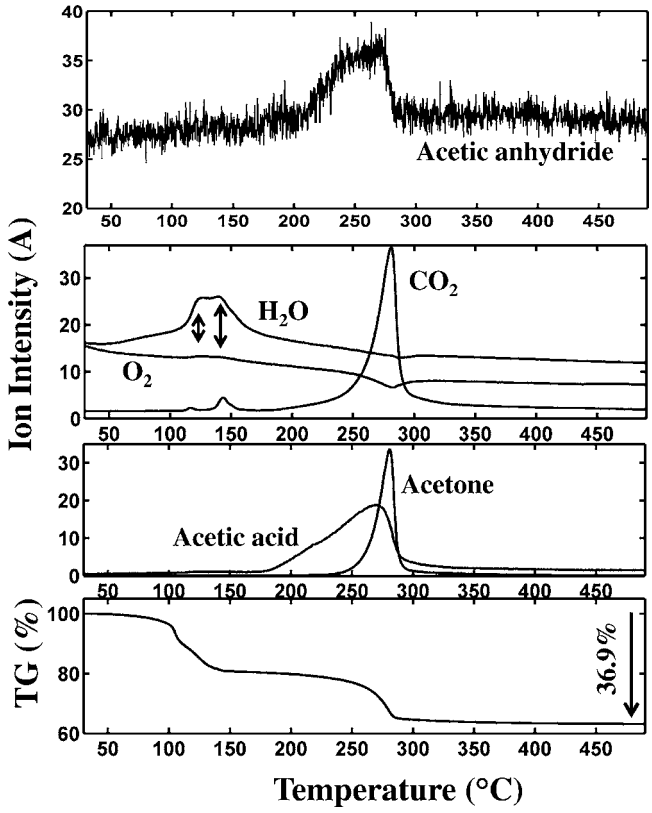

Figure 8. TGA–MS data produced by decomposition of aged zinc hydroxide acetate under an argon atmosphere at a heating rate of 3 °C/min. The ion intensities for CO_2, H_2O, O_2, acetic acid, acetone, and acetic anhydride are scaled by 10^{10}, 10^9, 10^{10}, 10^{12}, 10^{11}, and 10^{14}, respectively.

100 °C, and the maximum rate of water evolution was in the region 100–150 °C, where a small amount of carbon dioxide was also detected. Carbon dioxide, acetic acid, acetone, and traces of acetic anhydride were detected at temperatures greater than 200 °C. In the case where an exotherm was detected, maximum CO_2 evolution occurred at ~280 °C and was accompanied by consumption of O_2, indicating an oxidation process, which we assign to oxidation of acetic anhydride to CO_2 according to reaction (9). This conclusion is supported by a sudden drop in the mass spectrometer signal for acetic anhydride in this region; however, the formation of CO_2 and acetone can also be attributed to decomposition of molten $Zn(CH_3CO_2)_2$ [see reaction (8)].

Considering the data collected during the transformation of $Zn_5(OH)_8(CH_3CO_2)_2{\cdot}2H_2O$ to ZnO, we propose that $Zn_5(OH)_8(CH_3CO_2)_2{\cdot}2H_2O$ first undergoes dehydration according to reaction (2) in the temperature range of 25–93 °C with a mass loss of ~5.8%, which is in agreement with a predicted mass loss of 5.8% for the formation of anhydrous $Zn_5(OH)_8(CH_3CO_2)_2$ from the dihydrate. $Zn_5(OH)_8(CH_3CO_2)_2$ subsequently forms ZnO and $Zn(CH_3CO_2)_2$ with release of water [reaction (3)]. These findings are in agreement with data in previously reported work.[22]

The evolution of $Zn(CH_3CO_2)_2$ is integral to the discussion above, but the processes involved subsequent to reaction (3)

dx.doi.org/10.1021/ic302328e | Inorg. Chem. 2013, 52, 95–102

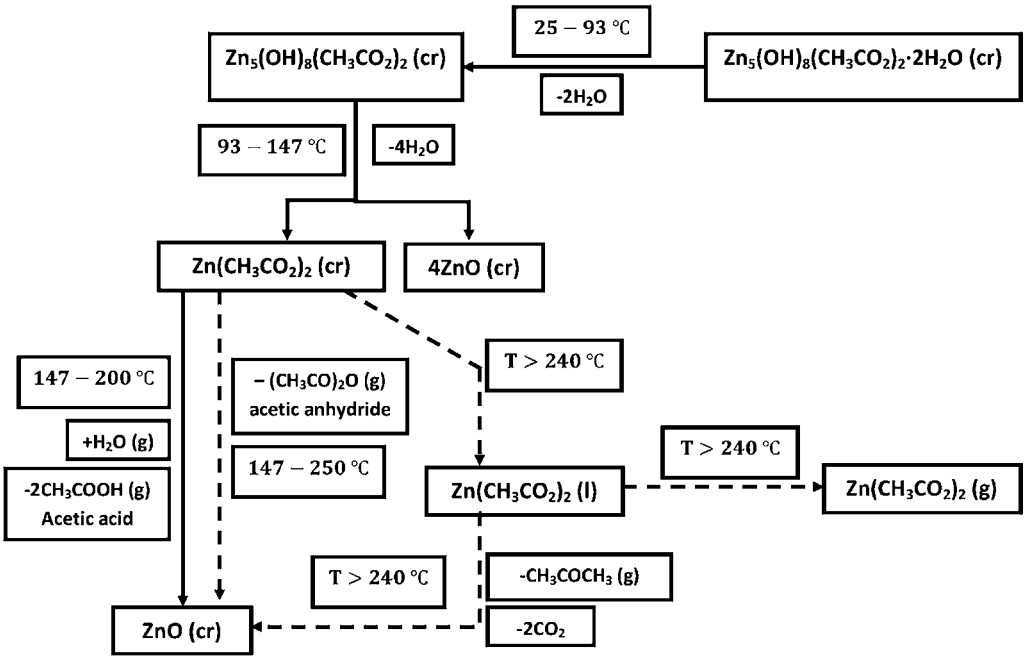

Figure 9. Thermal transformation of $Zn_5(OH)_8(CH_3CO_2)_2{\cdot}2H_2O$ to ZnO. Dotted lines indicate side reactions.

are not straightforward. The decomposition or volatilization behavior of $Zn(CH_3CO_2)_2$ upon heating is sensitive to the humidity of the surrounding atmosphere.[13,30] $Zn(CH_3CO_2)_2$ can form $Zn_4O(CH_3CO_2)_6$ and acetone upon heating in dry atmospheres,[31,32] and $Zn_4O(CH_3CO_2)_6$ may subsequently form ZnO, acetone, and CO_2 according to reaction (4).[31] In our studies, acetone and CO_2 were both detected by TGA–MS. Furthermore, upon heating, $Zn(CH_3CO_2)_2$ has been reported to form $Zn_4O(CH_3CO_2)_6$[31] together with acetic anhydride [$(CH_3CO)_2O$; reaction (5)], which was also detected in the current work.

$$Zn_4O(CH_3CO_2)_6(s) \xrightarrow{T>250\ ^\circ C} Zn_4O(CH_3CO_2)_6(l) \xrightarrow{T>250\ ^\circ C} 4ZnO(s) + 3CH_3COCH_3(g) + 3CO_{2(g)} \quad (4)$$

$$4Zn(CH_3CO_2)_2(s) \xrightarrow{180-250\ ^\circ C} Zn_4O(CH_3CO_2)_6(s) + (CH_3CO)_2O(g) \quad (5)$$

Another explanation for the presence of acetic anhydride is in reaction (6), although this may reflect a process similar to that shown in reaction (5), but where the intermediate $Zn_4O(CH_3CO_2)_6$ is not identified.

$$Zn(CH_3CO_2)_2(s) \xrightarrow{147-250\ ^\circ C} ZnO(s) + (CH_3CO)_2O(g) \quad (6)$$

In highly humid atmospheres, however, $Zn(CH_3CO_2)_2$ can react to form ZnO and acetic acid [reaction (7)],[30] which was also detected by us.

$$Zn(CH_3CO_2)_2 + H_2O \xrightarrow{147-200\ ^\circ C} ZnO + 2CH_3CO_2H \quad (7)$$

Anhydrous zinc acetate has a reported melting point of 240–250 °C[30,31] (see also the Supporting Information), and molten $Zn(CH_3CO_2)_2$ decomposes to ZnO, releasing acetone and CO_2 [reaction (8)], both of which were detected by TGA–MS. Oxidation of acetic anhydride to CO_2 and water is also possible according to reaction (9).[14] This is consistent with our MS data that show consumption of O_2 and a coincident reduction in the acetic anhydride signal with release of CO_2.

$$Zn(CH_3CO_2)_2(l) \xrightarrow{T>240\ ^\circ C} ZnO(s) + CH_3COCH_3(g) + CO_2(g) \quad (8)$$

$$(CH_3CO)_2O + 4O_2 \rightarrow 4CO_2 + 3H_2O \quad (9)$$

These insights reconcile our XRD data, which contain peaks assigned to only ZnO at temperatures >200 °C, with TGA–DTA and MS data that reveal processes occurring at temperatures >200 °C. We propose that molten materials such as $Zn(CH_3CO_2)_2$ and $Zn_4O(CH_3CO_2)_6$ are reacting in this temperature range.

Although there may be multiple reactions involved in this temperature region, the mass loss observed by TGA in zone 3 between 147 and 250 °C (14.7%) can be mainly assigned to processes that form ZnO, which is in agreement with the calculated mass loss for decomposition of anhydrous zinc acetate to ZnO from any possible route. However, there is a further 2.7% mass loss between 250 and 400 °C with an associated exothermic process at ~362 °C. We assign this to the release of volatile zinc-bearing material. Importantly, to our knowledge, the release of volatile material from zinc hydroxyacetate during the course of heating has not been reported. This issue may explain the range of reported waters of hydration in the literature. We examined this process in detail by heating zinc hydroxyacetate, which was first dehydrated at 150 °C for 1 h, in a sublimation apparatus at 350 °C for 4 h under vacuum. During this time, gas was evolved and the color of the powder changed from white to brown/gray. A whitish sublimate was deposited in the apparatus, and the sublimate and the nonvolatile reaction product were collected and analyzed by SEM and XRD. The nonvolatile product was

dx.doi.org/10.1021/ic302328e | Inorg. Chem. 2013, 52, 95–102

ZnO, as expected (see the Supporting Information). The XRD pattern of the sublimate contained peaks assigned to $Zn(CH_3CO_2)_2$ (JC-PDF 00-001-0089) and $Zn(CH_3CO_2)_2.2H_2O$ (JC-PDF 00-033-1464; see the Supporting Information). Interestingly, the volatile compound $Zn_4O(CH_3CO_2)_6$ has been reported to be formed by thermal decomposition of zinc acetate,[32−34] but no peaks in the XRD patterns recorded in the current work could be assigned to this compound. However, we cannot discount a reaction between any $Zn_4O(CH_3CO_2)_6$ that may have formed and gaseous acetic acid to produce zinc acetate[35] according to reaction (10).

$$Zn_4O(CH_3CO_2)_6 + 2CH_3CO_2H \rightarrow 4Zn(CH_3CO_2)_2 + H_2O \quad (10)$$

TGA−DTA experiments (see the Supporting Information) showed that pure zinc acetate dihydrate undergoes dehydration to form anhydrous $Zn(CH_3CO_2)_2$ with an associated 16.6% mass loss (cf. a theoretical value of 16.4%) at ∼50−100 °C. An endothermic peak at ∼250 °C is assigned to the melting of $Zn(CH_3CO_2)_2$, which then undergoes decomposition and/or volatilization with an exothermic peak located at ∼310 °C. The overall theoretical mass loss for decomposition of zinc acetate dihydrate to ZnO is 62.9%, but in a fashion similar to that of the zinc hydroxyacetate experiments, we observe more than expected mass loss (9.6%), which we attribute to volatilization of zinc-bearing materials. Furthermore, the heating rate affects the overall mass loss; TGA experiments with zinc acetate dihydrate with heating rates of 1 and 5 °C/min (see the Supporting Information) reveal extra mass loss values of 6.2% and 9.6%, respectively, which we assign to the volatilization processes. Although decomposition of pure zinc acetate may proceed differently from that generated during decomposition of zinc hydroxyacetate, there is sufficient evidence for us to conclude that volatile species are evolved during calcination of zinc hydroxyacetate. Including this extra mass loss component of 6.2−9.6% of the ∼20% of the ZnO formed via $Zn(CH_3CO_2)_2$ into TGA calculations to determine n, the waters of hydration, we conclude that $n = 2$.

On the basis of our experiments, we suggest that thermal decomposition of zinc hydroxyacetate dihydrate follows the scheme shown in Figure 9.

4. CONCLUSIONS

The reaction of aqueous zinc acetate with sodium hydroxide produced the layered compound $Zn_5(OH)_8(CH_3CO_2)_2{\cdot}2H_2O$, which was calcined to produce nanocrystalline ZnO. Calcination proceeds via a series of steps, starting with dehydration of $Zn_5(OH)_8(CH_3CO_2)_2{\cdot}2H_2O$, followed by decomposition of $Zn_5(OH)_8(CH_3CO_2)_2$ at the relatively low temperatures of 90−110 °C to form nanocrystals of ZnO and $Zn(CH_3CO_2)_2$. This low temperature of nucleation is the key feature that distinguishes the formation of ZnO by this process from others involving calcination and that is directly responsible for the very small particles produced. Decomposition and some volatilization of zinc acetate are then responsible for the processes at temperatures between 150 and 400 °C. Most of the zinc acetate in the presence of water vapor decomposes when heated to form ZnO and acetic acid, although other reactions can also be involved that produce CO_2, acetone, and acetic anhydride. A zinc-containing sublimate, presumed to be zinc oxyacetate $Zn_4O(CH_3CO_2)_6$, was also produced at over 250 °C, which is responsible for the excess of mass loss detected in TGA studies. No further chemical change occurs above 400 °C, but the height of the X-ray reflections for ZnO increase because of annealing of the crystal lattice until the temperature reaches about 550 °C.

■ ASSOCIATED CONTENT

Supporting Information

TGA−DTA on as-synthesized zinc hydroxyacetate materials and zinc acetate dihydrate, 3D-stacked XRD patterns showing decomposition of zinc hydroxyacetate against temperature, XRD patterns (low angle) for the products made by method B, TGA−DTA on the nonvolatile product of calcination of zinc hydroxyacetate, and TGA−MS data for experiments performed under an argon atmosphere. This material is available free of charge via the Internet at http://pubs.acs.org.

■ AUTHOR INFORMATION

Corresponding Author

*E-mail: michael.cortie@uts.edu.au. Phone: (+61)-2-9514-2208.

Notes

The authors declare no competing financial interest.

■ ACKNOWLEDGMENTS

This work was supported by PT. Indo Lysaght (Indonesia). We also thank Jean-Pierre Guerbois for assistance with TGA−MS, Dr. R. Wuhrer for electron microscopy, Dr. M. Berkahn for assistance with XRD studies, and Dr. K. Kannangara, School of Science and Health, UWS, for solid-state NMR. Part of this research was undertaken on the Powder Diffraction Beamline at the Australian Synchrotron, Victoria, Australia.

■ REFERENCES

(1) Warinner, W. D.; Conroy, E. H. Production of zinc oxysulfate. U.S. Patent 2,602,727, 1952.
(2) Westfall, D. G.; Amrani, M.; Peterson, G. A. *Better Crops* **1999**, *83* (2), 18−22.
(3) Moezzi, A.; McDonagh, A. M.; Cortie, M. B. *Chem. Eng. J.* **2012**, *185−186*, 1−22.
(4) Cordeiro, C. S.; Arizaga, G. G. C.; Ramos, L. P.; Wypych, F. *Catal. Commun.* **2008**, *9* (11−12), 2140−2143.
(5) Zieba, A.; Pacula, A.; Serwicka, E. M.; Drelinkiewicz, A. *Fuel* **2010**, *89* (8), 1961−1972.
(6) Bull, R. M. R.; Markland, C.; Williams, G. R.; O'Hare, D. *J. Mater. Chem.* **2010**, *21*, 6.
(7) Ozgur, U.; Ya, I. A.; Liu, C.; Teke, A.; Reshchikov, M. A.; Dogan, S.; Avrutin, V.; Cho, S. J.; Morkoc, H. *J. Appl. Phys.* **2005**, *98* (4), 041301.
(8) Klingshirn, C. *Phys. Status Solidi B* **2007**, *244* (9), 3027−3073.
(9) Moezzi, A.; Cortie, M.; McDonagh, A. *Dalton Trans.* **2011**, *40* (18), 4871−4878.
(10) Morioka, H.; Tagaya, H.; Kadokawa, J. I.; Chiba, K. *J. Mater. Sci. Lett.* **1999**, *18* (12), 995−998.
(11) Kandare, E.; Hossenlopp, J. M. *Inorg. Chem.* **2006**, *45* (9), 3766−3773.
(12) Cui, Q.; Yu, K.; Zhang, N.; Zhu, Z. *Appl. Surf. Sci.* **2008**, *254* (11), 3517−3521.
(13) Estruga, M.; Domingo, C.; Ayllón, J. A. *Eur. J. Inorg. Chem.* **2010**, *2010* (11), 1649−1654.
(14) Xia, Z.; Wang, Y.; Fang, Y.; Wan, Y.; Xia, W.; Sha, J. *J. Phys. Chem. C* **2011**, *115* (30), 14576−14582.
(15) Kawai, A.; Sugahara, Y.; Park, I. Y.; Kuroda, K.; Kato, C. Preparation of zinc oxide powders from 2-dimensional hydroxy-zinc complexes of basic zinc acetate, chloride and nitrate. In *Ceramic Transactions, Ceramic Powder Science IV*; Hirano, S., Messing, G. L.,

Hausner, H., Eds.; American Ceramic Society: Westerville, OH, 1991; Vol. *22*, pp 75−80.
(16) Morioka, H.; Tagaya, H.; Karasu, M.; Kadokawa, J.-i.; Chiba, K. *J. Mater. Res.* **1998**, *13* (4), 848−851.
(17) Hosono, E.; Fujihara, S.; Kimura, T.; Imai, H. *J. Colloid Interface Sci.* **2004**, *272* (2), 391−398.
(18) Poul, L.; Jouini, N.; Fievet, F. *Chem. Mater.* **2000**, *12* (10), 3123−3132.
(19) Wang, Y.; Li, Y.; Zhou, Z.; Zu, X.; Deng, Y. *J. Nanopart. Res.* **2011**, *13* (10), 5193−5202.
(20) Ye, F.; Peng, Y.; Chen, G.-Y.; Deng, B.; Xu, A.-W. *J. Phys. Chem. C* **2009**, *113* (24), 10407−10415.
(21) Zhang, Y.; Zhu, F.; Zhang, J.; Xia, L. *Nanoscale Res. Lett.* **2008**, *3* (6), 201−204.
(22) Biswick, T.; Jones, W.; Pacula, A.; Serwicka, E.; Podobinski, J. *Solid State Sci.* **2009**, *11* (2), 330−335.
(23) Kasai, A.; Fujihara, S. *Inorg. Chem.* **2006**, *45* (1), 415−418.
(24) Arizaga, G. G. C.; Satyanarayana, K. G.; Wypych, F. *Solid State Ionics* **2007**, *178* (15−18), 1143−1162.
(25) Morioka, H.; Tagaya, H.; Karasu, M.; Kadokawa, J.-i.; Chiba, K. *Inorg. Chem.* **1999**, *38* (19), 4211−4216.
(26) Song, R. Q.; Xu, A. W.; Deng, B.; Li, Q.; Chen, G. Y. *Adv. Funct. Mater.* **2007**, *17* (2), 296−306.
(27) Ye, B.-H.; Li, X.-Y.; Williams, I. D.; Chen, X.-M. *Inorg. Chem.* **2002**, *41* (24), 6426−6431.
(28) Kumar, U.; Thomas, J.; Thirupathi, N. *Inorg. Chem.* **2010**, *49* (1), 62−72.
(29) Hunt, P. A.; Straughan, B. P.; Ali, A. A. M.; Harris, R. K.; Say, B. J. *J. Chem. Soc., Dalton Trans.* **1990**, *7*, 2131−2135.
(30) Arii, T.; Kishi, A. *Thermochim. Acta* **2003**, *400* (1−2), 175−185.
(31) McAdie, H. G. *J. Inorg. Nucl. Chem.* **1966**, *28* (12), 2801−2809.
(32) Gyani, A. K.; Khan, O. F. Z.; O'Brien, P.; Urch, D. S. *Thin Solid Films* **1989**, *182* (1−2), L1−L4.
(33) Auger, V.; Robin, I. *C. R. Hebd. Seances Acad. Sci.* **1924**, *178*, 1546−1548.
(34) Hiltunen, L.; Leskela, M.; Makela, M.; Niinisto, L. *Acta Chem. Scand., Ser. A* **1987**, *A41* (10), 548−55.
(35) Gordon, R. M.; Silver, H. B. *Can. J. Chem.* **1983**, *61* (6), 1218−1221.

■ NOTE ADDED AFTER ASAP PUBLICATION

Figure 9 was incorrect in the version published ASAP on December 18, 2012; the correct version reposted on December 20, 2012.